Kinetics and Mechanism of the BrO Self-Reaction: Temperature- and Pressure-Dependent Studies

Matthew H. Harwood, David M. Rowley,* R. Anthony Cox, and Roderic L. Jones

Centre for Atmospheric Science, University Chemical Laboratory, Lensfield Road, Cambridge, CB2 1EW, U.K.

Received: October 8, 1997; In Final Form: December 30, 1997

The flash photolysis/UV absorption technique has been used to study the self-reaction of BrO radicals over the temperature range 222−298 K and the pressure range 100−760 Torr of N_2 or O_2. Two chemical sources of BrO radicals were used: photolysis of Br_2 in the presence of excess ozone and photolysis of O_2 in the presence of excess Br_2. The overall rate constant, k_1, for the BrO self-reaction (defined by $-d[BrO]/dt = 2k_1[BrO]^2$) was found to be temperature and pressure independent at $T \geq 250$ K, with $k_1 = (2.88 \pm 0.20) \times 10^{-12}$ cm^3 molecule^{-1} s^{-1}. At temperatures below 250 K, k_1 was found to be pressure dependent, due to the emergence of a new termolecular channel of the BrO self-reaction 1c, −1c forming the BrO dimer, Br_2O_2 ($BrO + BrO + M \rightleftharpoons Br_2O_2 + M$). Channel-specific rate constants were determined for the two bimolecular channels of the BrO self-reaction above 250 K, giving for (1a) ($BrO + BrO \rightarrow 2Br + O_2$) $k_{1a} = (5.31 \pm 1.17) \times 10^{-12} \exp\{(-211 \pm 59)/T\}$ cm^3 molecule^{-1} s^{-1} and for (1b) ($BrO + BrO \rightarrow Br_2 + O_2$) $k_{1b} = (1.13 \pm 0.47) \times 10^{-14} \exp\{(983 \pm 111)/T\}$ cm^3 molecule^{-1} s^{-1}. Below 250 K, the overall rate coefficient of the two bimolecular channels is reduced as the dimer forming channel emerges. At 235 and 222 K, rate constants for the formation (k_{1c}) and decomposition (k_{-1c}) of Br_2O_2 were recorded. Using the values for K_{1c}, ΔH_r for reaction 1c was estimated as -58.6 ± 0.1 kJ mol^{-1}. A UV absorption spectrum attributed to Br_2O_2 was also recorded over the wavelength range 300−390 nm. The cross section of the smooth Br_2O_2 spectrum was found to be 1.2×10^{-17}cm^2 molecule^{-1} at 320 nm. These results are rationalized in terms of a mechanism of the BrO self-reaction that shows competition, at low temperatures, between collisional quenching and unimolecular dissociation of an excited BrOOBr* intermediate. The rate constant for the reaction of oxygen atoms with molecular bromine was also determined in the course of these experiments [$O + Br_2 \rightarrow BrO + Br$ (5)], giving $k_5 = (5.12 \pm 1.86) \times 10^{-13} \exp\{(989 \pm 91)/T\}$ cm^3 molecule^{-1} s^{-1}. All errors are 1σ. The atmospheric implications of these results are discussed.

Introduction

The BrO radical is an important intermediate in the atmospheric breakdown of bromine-containing compounds and is involved in several cycles leading to the destruction of atmospheric ozone. The reaction between BrO and ClO is an important contributor to stratospheric ozone loss in both polar regions and midlatitudes.[1] In addition, in the tropospheric marine boundary layer in Arctic regions during springtime, large concentrations of BrO have been observed,[2] and concomitant losses of ozone have been attributed to the chemistry of BrO.

Considering the importance of BrO in the atmosphere, there remain uncertainties in the kinetics and mechanisms of its gas-phase reactions, such as the self-reaction of BrO radicals. This reaction may well play a part in ozone loss in the troposphere[3] and must also be taken into account when studying other reactions of BrO (e.g., the atmospherically crucial $BrO + HO_2$ and $BrO + ClO$ reactions) in the laboratory. In this paper we present a study of the self-reaction of BrO as a function of pressure and temperature in an attempt to increase the understanding of this process. This paper continues from the work of Rowley et al.,[4] in which the BrO self-reaction was studied at room temperature.

There have been numerous previous studies of the BrO self-reaction,[5−16] indicating that the reaction proceeds by two channels: one producing atomic bromine (1a) and the other producing molecular bromine (1b). The most recent recommendation DeMore et al.[17] gives the following Arrhenius expressions for the two channels that are used in current chemical models of the atmosphere.

$$BrO + BrO \rightarrow Br + Br + O_2 \qquad k_{1a} = 2.4 \times 10^{-12} \exp(40/T) \quad (1a)$$

$$BrO + BrO \rightarrow Br_2 + O_2 \qquad k_{1b} = 2.8 \times 10^{-14} \exp(860/T) \quad (1b)$$

The experimental evidence for this two-channel mechanism is strong. Previous studies have determined the overall rate constant for reaction 1 ($k_1 = k_{1a} + k_{1b}$) by monitoring the second-order kinetic decay of photochemically produced BrO by UV−visible absorption spectroscopy (AS) or mass spectrometry (MS). In other studies, production of BrO in the presence of excess ozone allowed the rate of channel (1b) only to be measured due to the rapid regeneration of BrO through the reaction of Br, formed in channel 1a, with O_3:

$$Br + O_3 \rightarrow BrO + O_2 \quad (2)$$

which leads to the "masking" of channel 1a. In addition, studies of the quantum yields for Br_2-photosensitized decomposition

* To whom correspondence should be addressed. E-mail: rowley@atm.ch.cam.ac.uk.

S1089-5639(97)03264-7 CCC: $15.00
Published on Web 02/14/1998

of ozone (e.g., ref 10) have been used to determine the branching ratio $k_{1a}/(k_{1a} + k_{1b})$.

While most studies of the BrO self-reaction have measured the rate of disappearance of BrO, there have been some direct studies of the reaction products. The formation of Br_2 in this system was observed both by emission from electronically excited Br_2[7] and by MS,[12] and kinetic parameters for channel 1b have been determined directly by monitoring the production of Br_2 in reaction 1 by MS[13] and by AS.[16] While Br atoms themselves have not been directly observed as products from reaction 1, their production has been inferred from the concomitant consumption of ozone in reaction 2 (e.g., ref 6).

The temperature dependence of k_1 has been studied by three groups: Sander and Watson,[6] Turnipseed, Birks, and Calvert,[12] and Mauldin, Wahner, and Ravishankara.[5] The first two studies showed excellent agreement for k_1, exhibiting a slightly negative temperature dependence. In addition, Sander and Watson found k_1 to be independent of pressure in the range 50−475 Torr. The agreement with the work of Turnipseed, Birks, and Calvert at 2 Torr total pressure supports this finding above 253 K (the lowest T of Turnipseed et al.'s work). However, at lower temperature (220 K), Mauldin, Wahner, and Ravishankara report a pressure dependence for k_1 in contrast with the study of Sander and Watson.

The observation of a negative temperature dependence for channel (1b), and a pressure dependence for k_1 and k_{1b},[5] strongly suggest that reaction 1 proceeds via a complex-forming bimolecular mechanism. Radical−radical reactions of this type often proceed on attractive potential energy surfaces. One proposed mechanism[5] involves the formation of a vibrationally excited intermediate (Br_2O_2*):

$$BrO + BrO \rightleftharpoons Br_2O_2^*$$

$$Br_2O_2^* + M \rightleftharpoons Br_2O_2 + M$$

$$Br_2O_2 \rightarrow BrOO + Br$$

$$Br_2O_2^* \rightarrow BrOO + Br$$

$$Br_2O_2 \rightarrow Br_2 + O_2$$

$$Br_2O_2^* \rightarrow Br_2 + O_2$$

$$BrOO \rightarrow Br + O_2$$

Owing to the paucity of temperature- and pressure-dependent studies of this reaction, it is still not clear whether channels 1a and 1b proceed directly or via the Br_2O_2* intermediate which has sufficient lifetime to be collisionally stabilized, or indeed by both mechanisms. It is also possible that the dimer of BrO may exist as a stable product of the reaction at low temperatures as is the case in the ClO self-reaction (e.g., ref 18). There is some evidence for the collisionally stabilized Br_2O_2 species; Mauldin et al.[5] observed a transient, spectrally smooth absorber in a flash photolysis study of the BrO self-reaction at low temperatures which they assigned to the BrO dimer.

In this work, we have attempted to elucidate the kinetics and mechanism of the self-reaction of BrO radicals through a detailed study of the temperature and pressure dependence of the reaction. This study makes use of a recently developed apparatus for gas-phase kinetics which allows more rapid time-resolved absorption spectroscopy of transient species than has hitherto been possible in such studies.[4]

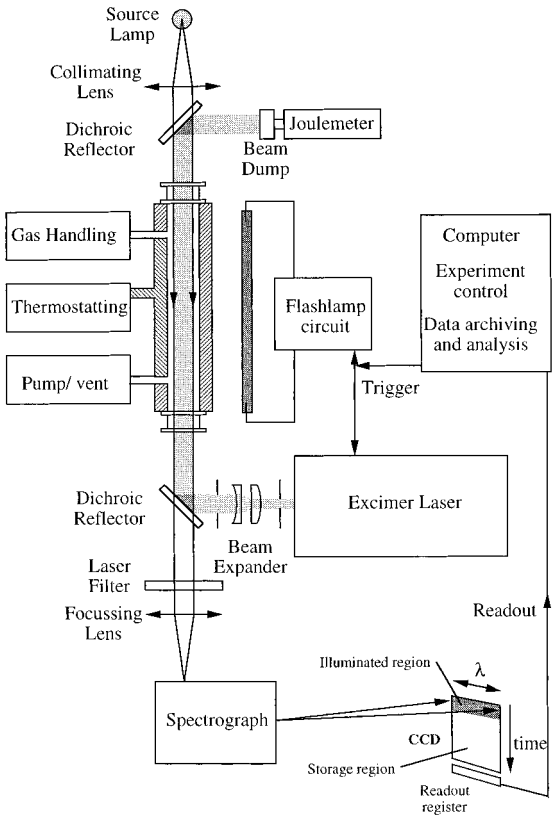

Figure 1. Schematic diagram of the apparatus used in this study. Source lamp light, having passed through the reaction cell, is dispersed and imaged across the top rows of the 2-dimensional CCD array. Charge shifting is then used to move the signal generated by incident light, into the storage region of the device, thereby recording rapid, sequential spectra. The excimer laser beam counterpropagates the source light beam.

Experimental Section

The experimental technique used for the work described here was flash photolysis with time-resolved UV−visible spectroscopy. Charged-coupled-device (CCD) detection was used to monitor the decay or evolution of chemical species. The apparatus has been described in detail previously,[4] and a brief summary is given here along with a full description of the recently installed laser photolysis system. A schematic diagram of the apparatus is shown in Figure 1.

Gas mixtures were prepared in a gas manifold using calibrated mass flow controllers (MKS 1159B) and glass "rotameter" flow meters (Glass Precision Engineering Ltd. RS1-3). These mixtures were made to flow into a triple-jacketed quartz reaction cell whose temperature could be regulated in the range 200−350 K to within 0.5 K using flowing liquid (Galden HT90 perfluoroether) from a recirculating unit (Huber HS80). Gases were pumped through the cell, where necessary, allowing cell pressures in the range 50−760 Torr to within 1 Torr to be maintained. Reaction initiation was achieved by photolysis using one of two light sources: a xenon flashlamp (Q-Arc Ltd.) placed adjacent and parallel to the reaction cell giving ca. 500 J/pulse of wavelengths 180−700 nm or an excimer laser. The laser (Lambda-Physik COMPex 200) was operated at 193 nm and gave pulse energies from 200 to 400 mJ/pulse. The laser

TABLE 1: Absorption Cross Sections for Measurement of Detected Species

absorber	cross sections[a] cm^2 $molecule^{-1}$ (λ/nm)	resolution (fwhm)/nm	temp available/K	detection limit/ molecules cm^{-3}	ref
BrO	1.55×10^{-17} (338.66)[b]	0.4	298, 228, 213	1×10^{11}	21
O_3	3.83×10^{-18} (280)	0.1	295, 243, 220	2×10^{12}, 5×10^{15} [c]	22
Br_2	3.02×10^{-19} (380)		*e*	1×10^{14}	23
Br_2O	2.06×10^{-18} (310)	0.6	298	1×10^{14}	24
OBrO	1×10^{-17} [d] (495.5)	1.7	298	1×10^{12}	4

[a] Values are quoted at a single wavelength at the source resolution as a guide to the cross section used. Species concentrations were determined by spectral fitting across a range of wavelengths, using "differential fitting" for structured spectra. See text for details. [b] Peak of the ($7 \leftarrow 0$) band. [c] Detection limits given respectively for the Hartley band and the Huggins bands. [d] Cross sections as assumed in Rowley et al.[4] [e] Parametrized.

beam was passed longitudinally through the reaction cell. The beam exiting the laser was collimated and beam expanded horizontally using a pair of fused silica cylindrical lenses (Exitech Ltd.) and steered along and out of the reaction cell using dichroic reflectors (Exitech Ltd.) on precision gimbal mounts (Melles Griot Ltd.). The laser beam filled the internal diameter of the cylindrical reaction cell. The laser beam energy was monitored both at the laser exit (Lambda-Physik internal powermeter) and at the beam dump using a joulemeter (Molectron Ltd.). Careful checks were made to ensure that no significant longitudinal concentration gradients of the photolytically generated species were produced in the reaction vessel.

The concentrations of precursor gases, reacting species, and products within the cell were measured by UV−visible absorption spectroscopy. Analysis light, from a 30 W continuous xenon lamp (Q-Arc Ltd.), was passed once through the 1 m reaction cell, dispersed, and imaged, using a 0.25 m astigmatic spectrograph (Chromex 250IS) onto the optical detector. The detector used was a 2-dimensional charged coupled device array (EEV CCD05-10-0-202) consisting of 1152 (rows) by 298 (columns) of detectors (pixels) which was masked so that only the top 30 rows of pixels were exposed to incident light. The spectrum of the analysis light was imaged across the top, exposed, pixels of the CCD array, and charge transfer was used to move signal into the masked region of the device to record time-resolved sequential spectra. After each experiment the signals were digitized and transferred to a personal computer for averaging and analysis.

Two types of spectral analysis were performed: absorbance spectra of gas mixtures in the reaction cell without photolysis were produced by ratioing equivalent spectra from successive CCD exposures with and without the gas mixture present, using Beer's law. For photolysis experiments, the flashlamp or laser was operated during the recording of sequential time-resolved spectra, and each time-resolved spectrum was ratioed to the average preflash intensity to calculate absorbance. In this case, postflash spectra show *changes* in the absorbance bought about by the photolysis flash and subsequent chemistry.

Postflash spectra were analyzed by numerically fitting cross sections for the species of interest to each observed postflash absorption spectrum as described previously.[4] Where the species of interest had structured absorption spectra, differential spectra were produced by appropriate filtering,[19] and similarly filtered reference spectra were fitted to the observed differential absorption, using the least-squares technique. As many of the rate parameters measured are linearly dependent upon the values of the absorption cross sections used, careful attention was paid to ensure that accurate cross sections were used. Reference cross sections were either measured or taken from the literature.

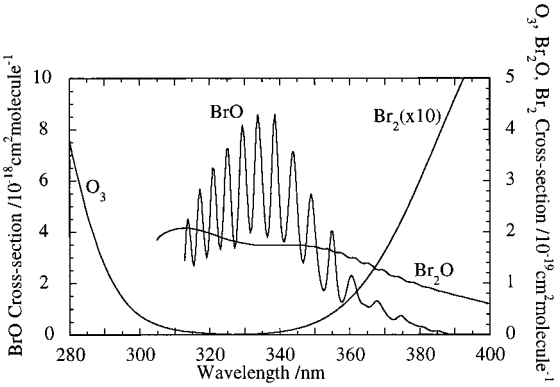

Figure 2. Reference absorption spectra of BrO, O_3, Br_2O, and Br_2 used in the spectral fitting, shown at the instrumental resolution of 1.7 nm fwhm.

Before use, literature cross sections were subject to several adjustments to account for differences in the conditions under which they were recorded and those employed in this work. Such adjustments, which have been described previously,[4,20] included smoothing of literature spectra to match the instrument function recorded in this work, recalibration of literature spectra onto the wavelength grid recorded in this work (which was determined using a Hg/Zn/Cd lamp), and wavelength shifting the literature spectra by very small degrees (usually <0.1 nm) in order to further optimize the fit to recorded spectra. The quality of the fit of literature to experimental spectra was very sensitive to the exact wavelength alignment of the two spectra, particularly for structured spectra, and wavelength shifts were necessary to account for small drifts in the wavelength calibration of the spectrograph during the course of experiments. Additionally, in this study, temperature-dependent absorption cross sections of species were used where appropriate. Where temperature-dependent spectra were not available, suitable interpolation between available data was used to generate spectra at the appropriate temperature.

In this work, a 150 grooves/mm grating was used with 50 μm wide spectrograph inlet slits. This gave a total spectral coverage of 130 nm at a resolution of 1.7 nm fwhm. The cross sections used for all the species monitored in this study and their sources are described in Table 1, and the reference spectra of BrO, Br_2, Br_2O, and O_3 are shown in Figure 2. Typical detection limits for each species using differential fitting over a convenient spectral range, for a signal-to-noise ratio of 1, are also given in Table 1.

Two distinct chemical sources of BrO radicals were used in this study. In the first, the xenon flashlamp was used to photolyze Br_2 [$(1-5) \times 10^{16}$ cm^{-3}] in the presence of excess

ozone [(5−100) × 10^{16} cm^{-3}], with the photolytically produced Br atoms reacting rapidly with ozone to produce BrO:

$$Br_2 + h\nu \rightarrow Br + Br \quad (3)$$

$$Br + O_3 \rightarrow BrO + O_2 \quad (2)$$

In this system, a Pyrex sleeve was placed around the flashlamp to prevent transmission of photolysis light at wavelengths <300 nm and thus prevent significant photolysis of ozone. Experiments verified that this was the case: ozone concentrations were unchanged within our detection limits (2 × 10^{12} cm^{-3}) when flashing O_3/N_2 mixtures.

In the second radical generation system, the excimer laser was used to photolyze molecular oxygen [bath gas: (0.2−3.3) × $10^{19}$$cm^{-3}$] in the presence of excess bromine [(1−20) × 10^{16} cm^{-3}]:

$$O_2 + h\nu \rightarrow O(^3P) + O(^3P) \quad (4)$$

$$O(^3P) + Br_2 \rightarrow BrO + Br \quad (5)$$

In both systems, BrO generation took place rapidly relative to the time scale of its subsequent removal. Typically, initial concentrations of BrO between 5 × 10^{13} and 4 × 10^{14} cm^{-3} were generated, in carrier flows of oxygen/nitrogen (in the Br_2 photolysis system) or oxygen (in the O_2 photolysis system). Experiments in both systems were carried out over the temperature range 222−298 K and from 100 to 760 Torr total pressure.

Bromine (BDH, stated purity >99.9%) was degassed several times using successive freeze−pump−thaw cycles prior to use. Nitrogen (Distillers MG, >99.995%) and oxygen (Distillers MG, >99.99%) were used as supplied. Ozone was prepared as required by passage of oxygen through a discharge ozonizer (Argentox GL10).

The use of separate chemical systems for the generation of BrO radicals in this work allowed different aspects of the reaction system to be investigated. Results from each system are therefore presented separately.

Results

Photolysis of Br_2 in the Presence of O_3. The decay of BrO radicals by their self-reaction is expected to be second-order kinetically. Moreover in the presence of excess ozone, any bromine atoms produced in channel 1a of the BrO + BrO reaction are rapidly reconverted into BrO by reaction with ozone. Consequently, this channel has no effect on the observed BrO kinetics, and the observed BrO decay represents channel (1b) only, as has been verified in several previous studies:[4−14]

$$-d[BrO]/dt = 2k_{1b}[BrO]^2 \quad (i)$$

However, as described by Rowley et al.,[4] there are certain complications to this reaction system. At room temperature and with very low (<10^{-4}) [BrO]/[O_3] ratios, the reaction between BrO and O_3 occurs, producing OBrO:

$$BrO + O_3 \rightarrow OBrO + O_2 \quad (6)$$

This reaction disturbs the "pure" second-order nature of the BrO decay and adds a first-order component. In addition, at high (>10^{-3}) [BrO]/[O_3] ratios (although keeping ozone in excess), the reaction between Br atoms and BrO (7) (and to some extent the Br self-reaction (8)) can remove some of the Br atoms formed in channel 1a without regeneration of BrO, effectively allowing this channel to contribute partially to the BrO decay.

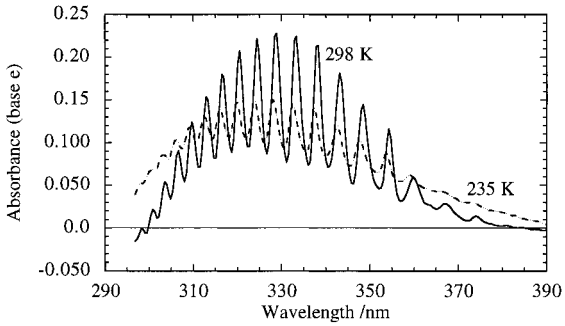

Figure 3. Postflash absorption spectra generated following flashlamp photolysis of $Br_2/O_3/O_2$ mixtures at 298 and 235 K. Spectra are generated relative to preflash intensities and therefore represent *changes* in absorption bought about by the photolysis flash and subsequent chemistry.

$$Br + BrO\ (+M) \rightarrow Br_2O\ (+M) \quad (7)$$

$$Br + Br + M \rightarrow Br_2 + M \quad (8)$$

Furthermore, the reaction between Br atoms and ozone (3) has a positive temperature dependence[17] whereas that between Br and BrO accelerates rapidly at low temperatures.[26] Thus, experiments carried out in this work at low temperatures were performed with concentrations of ozone high enough to ensure that any Br atoms formed in channel 1a were consumed by ozone and not by BrO. It was unavoidable, however, that high instantaneous concentrations of Br and BrO coexisted immediately after the flash, and some Br_2O was formed in this period, particularly at the lowest temperatures. Numerical simulation of the reaction system using FACSIMILE[25] showed that, under all experimental conditions used in this work, the Br_2O formed in the flash would play no further part in the kinetics. To verify this, Br_2O was monitored as a function of time by virtue of its vibrational structure between 350 and 380 nm, and as expected, the concentration of Br_2O, once formed, remained constant, [Br] being too low after the photolysis flash to form further Br_2O or to remove it in reaction 9:[4]

$$Br + Br_2O \rightarrow Br_2 + BrO \quad (9)$$

The use of low [BrO]/[O_3] ratios to limit Br_2O formation raised the possibility that the reaction between BrO and O_3 might affect the kinetic decay of BrO at low temperatures. As shown by Rowley et al.,[4] at 298 K ozone concentrations in excess of 10^{17} molecules cm^{-3} led to production of observable OBrO and a measurable deviation of BrO decay traces from second order. Experiments were therefore performed here at 235 K with deliberately low [BrO]/[O_3] ratios to determine whether any OBrO was formed. In contrast to the 298 K work, no characteristic OBrO absorption was observed, and possible complications from the BrO + O_3 reaction were discounted. This is in accordance with the work of Rattigan et al.,[15] which suggests that reaction 6 has a substantial positive temperature dependence.

Experiments were performed at a range of pressures between 100 and 760 Torr and at the temperatures 298, 267, 250, 235, and 222 K. A typical postflash spectrum recorded from an experiment at 298 K is shown in Figure 3. The spectrum shows the positive characteristically structured absorption due to the BrO formed and the negative absorption from the O_3 consumed by the photolytically generated Br atoms. Spectral fitting to successive postflash spectra gave the variation of BrO with time

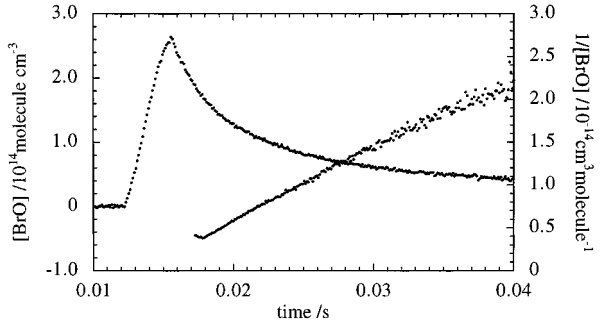

Figure 4. Temporal variation of [BrO] determined by fitting the BrO spectral structure to successive spectra recorded by the CCD. The trace shows BrO buildup and decay following flashlamp photolysis of $Br_2/O_3/O_2$ mixtures at 298 K. Also shown is the corresponding second-order plot (1/[BrO] vs time) for these data.

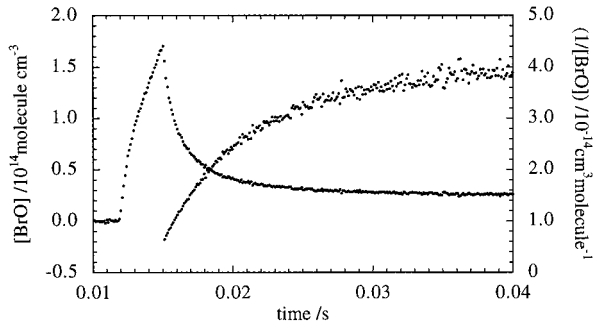

Figure 5. BrO buildup and decay trace following flashlamp photolysis of $Br_2/O_3/O_2$ mixtures at 235 K. Also shown is the corresponding second-order plot (1/[BrO] vs time) for these data, which shows distinct nonlinearity.

as shown in Figure 4. These decays were analyzed to determine the rate constant k_{1b}. The integrated form of the rate eq i was used

$$\frac{1}{[\mathrm{BrO}]_t} = \frac{1}{[\mathrm{BrO}]_0} + 2k_{1b}t \qquad \text{(ii)}$$

1/[BrO] was plotted against t, giving a slope equal to $2k_{1b}$. Figure 4 shows a typical decay trace recorded at room temperature and the associated second-order plot.

The decay of BrO was found to be second order at room temperature, and the slopes of the second-order plots were found to be independent of pressure in the range 100−760 Torr. The mean value of the second-order rate coefficient, k_{1b}, at 298 K was $(3.12 \pm 0.12) \times 10^{-13}$ cm^3 molecule^{-1} s^{-1}. At lower temperatures, the initial rate of decay of BrO increased and below 250 K, the BrO decays were found to lose their second-order nature. Figure 5 shows a typical BrO decay recorded at 235 K and the corresponding second-order plot which shows distinct nonlinearity. As the temperature was lowered, this deviation from second-order behavior increased, and an underlying absorption was detected in the postflash spectra. This is clear in Figure 3, where a postflash spectrum at 235 K is compared to one recorded at 298 K.

Figure 6 shows postflash spectra recorded at 235 K from three discrete times after the flash, the spectral contribution from BrO having been subtracted. This underlying absorption spectrum consists of the contribution of the Br_2O formed in the initial postflash chemistry, the O_3 removed (negative), and a spectrally smooth unknown absorber which decays with time.

Mauldin et al.[5] also observed an underlying absorption in their studies of the BrO self-reaction at low temperature; however, they observed no deviation from second-order kinetic behavior.

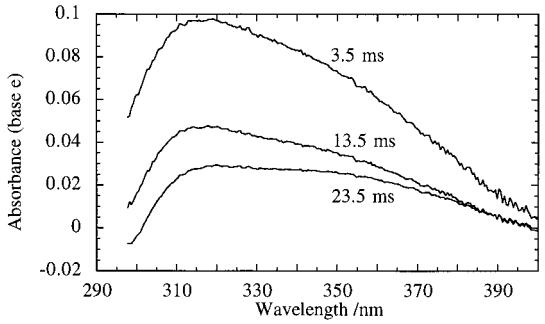

Figure 6. Postflash spectra obtained at three different reaction times (in ms) after the flashlamp photolysis of $Br_2/O_3/O_2$ mixtures at 235 K. The spectral contribution of BrO has been subtracted from these spectra.

As pointed out in their study, there are only two obvious candidates for this new absorber: BrOO and Br_2O_2. Mauldin et al. photolyzed Br_2 in O_2 and saw no evidence for the BrOO species. This experiment was repeated here at 235 K, and similarly no absorption in the range 270−390 nm was observed. (BrOO by analogy with ClOO would be expected to have a strong absorption spectrum in this region.) While these negative results could mean that BrOO is not stable at this temperature, we have modeled this reaction system with FACSIMILE, using the rates for the chlorine analogues of reactions 10 and 11.[17] The results show that the quantity of BrOO formed would be expected to be below our detection limits anyway, if the reaction between Br and BrOO is as fast as the Cl + ClOO reaction and if BrOO and ClOO have similar absorption cross sections.

$$\mathrm{Br} + \mathrm{O_2} \rightleftharpoons \mathrm{BrOO} \qquad (10)$$

$$\mathrm{Br} + \mathrm{BrOO} \rightarrow \mathrm{Br_2} + \mathrm{O_2} \qquad (11)$$

Further experiments were therefore performed in which Br_2 was photolyzed in O_3 where the bath gas was changed from being all O_2 to being predominantly (99%) N_2. In both cases, the same unknown spectrum was observed, and the absorption showed the same temporal behavior, suggesting that the unknown absorbing species was not involved in the equilibrium step 10.

Considering this evidence against the new species being BrOO and, by analogy with the ClO + ClO reaction, we conclude that the most likely candidate for the new absorber is the BrO dimer (Br_2O_2). Inclusion of a reversible termolecular reaction between BrO and BrO, giving the dimer (1c),

$$\mathrm{BrO} + \mathrm{BrO} + \mathrm{M} \rightleftharpoons \mathrm{Br_2O_2} + \mathrm{M} \qquad (1c,-1c)$$

into the reaction scheme in the FACSIMILE model allowed the complex kinetic decay of BrO to be successfully fitted. The rate constants returned by FACSIMILE for reactions 1b and 1c were highly correlated, however, and the approach used by Nickolaisen et al.[18] in their analysis of ClO self-reaction kinetics was therefore adopted. The experiments were performed as a function of pressure, and the initial slopes of the second-order plots were measured to give a value for the overall initial second-order removal of BrO (k_{init}) before sufficient Br_2O_2 had built up for the reverse reaction −1c to affect the BrO decay. In this case the initial decay of BrO should be given by

$$-\frac{\mathrm{d[BrO]}}{\mathrm{d}t} = 2(k_{init})[\mathrm{BrO}]^2 \qquad \text{(iii)}$$

where $k_{init} = (k_{1b} + k_{1c}[\mathrm{M}])$. The values of k_{init} were plotted as a function of [M] for all temperatures studied here, and all plots

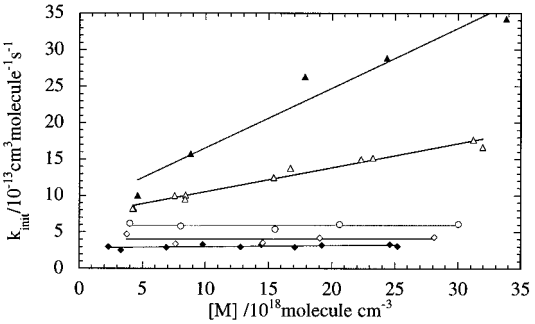

Figure 7. Plot of k_{init} vs [M] for the initial second-order decay of BrO after the flashlamp photolysis of $Br_2/O_3/O_2$ mixtures at all temperatures studied here: filled diamonds, 298 K; open diamonds, 267 K; open circles, 250 K; open triangles, 235 K; filled triangles, 222 K.

TABLE 2: Rate Coefficients for BrO + BrO Reaction from the Br_2 Photolysis System

T/K	k_{1b}[a]/10^{-13} cm^3 molecule^{-1} s^{-1}	k_{1c}[a]/10^{-32} cm^6 molecule^{-2} s^{-1}	k_{-1c}[a]/10^{-18} cm^3 molecule^{-1} s^{-1}	K_{1c}[a]/10^{-14} cm^3 molecule^{-1}
298	3.12 ± 0.1			
267	4.32 ± 0.1			
250	5.93 ± 0.3			
235	6.82 ± 0.3	3.6 ± 0.2	5.8 ± 3.0	0.62 ± 0.3
	(3.2 ± 5.0)[b]	(20 ± 44)		
222	8.3 ± 2.2	8.2 ± 1.1	2.5 ± 0.5	3.3 ± 0.8
	(−5.2 ± 4.9)	(77 ± 51)		

[a] All errors are 1σ. [b] Values in brackets are obtained from a three-parameter fit to the k_{init} data of the form $k_{init} = k_{1b} + k_{1c}[M]/(1 + (k_{1c}[M]/k_\infty))0.6^{\{1+[\log(k_{1c}[M]/k_\infty)]^2\}^{-1}}$.

are shown in Figure 7. No statistically significant pressure dependence was observed in the data at 298, 267 and 250 K, but at 235 and 222 K, the values of k_{init} were pressure-dependent. The pressure dependence of k_{init} at 222 K is stronger than that at 235 K and shows distinct curvature. The data were analyzed initially with the assumption that both k_{1b} and k_{1c} are pressure-independent, i.e., that the bimolecular channel is independent of pressure and that the termolecular channel does not exhibit falloff. The values of k_{1b} and k_{1c} so obtained are given in Table 2. Above 250 K, k_{1b} shows Arrhenius behavior with $k_{1b} = (1.13 \pm 0.47) \times 10^{-14} \exp[(983 \pm 111)/T]$ cm^3 molecule^{-1} s^{-1}.

To obtain the rate of dimer decomposition at 222 and 235 K, FACSIMILE was used to fit the entire decay trace and optimize k_{-1c} with k_{1b} and k_{1c} fixed at the values determined using k_{init}. However, it was found that while the initial rates of the decay were invariant with the ozone concentration, the decay traces at longer times changed their nature with changing ozone concentrations. As the ozone concentration was reduced, the decays approached second order. This effect was attributed to the reaction between Br atoms and Br_2O_2 which, by analogy with Cl + Cl_2O_2, is likely to be very fast and have the effect of catalytically converting Br_2O_2 to O_2 and Br_2:

$$Br + Br_2O_2 \rightarrow BrOO + Br_2 \qquad (12)$$

$$BrOO \rightarrow O_2 + Br \qquad (-10)$$

$$\text{net:} \qquad Br_2O_2 \rightarrow O_2 + Br_2$$

To investigate the effect of secondary reactions of bromine atoms, experiments were performed to monitor the decay of BrO as a function of ozone concentration ($(1-4) \times 10^{17}$ molecules cm^{-3}) under otherwise identical conditions. Care was taken to ensure that the Br_2 concentration, and therefore the initial concentration of photochemically generated bromine atoms, $[Br]_0$, were unchanged. For a given $[Br]_0$, the amount of BrO produced depends upon the relative rates of the reaction of Br with O_3 (reaction 2) and the reaction of Br with BrO (reaction 7). Experimentally, more BrO was observed at higher ozone concentrations and analysis of the variation of $[BrO]_{max}$ with $[O_3]$ at 235 K and 760 Torr gave $k_7 = (9.1 \pm 2.0) \times 10^{-12}$ cm^3 molecule^{-1} s^{-1}, which compares reasonably well with that of Hayman et al.[26] of $(6.5 \pm 3.5) \times 10^{-12}$ cm^3 molecule^{-1} s^{-1}. To obtain an estimate for the rate of reaction between Br and Br_2O_2, the decay traces from these experiments were analyzed simultaneously using FACSIMILE, allowing $[Br]_0$, k_{-1c}, and k_{12} to optimize. This showed that reaction 12 is indeed rapid, with an average optimized value of $k_{12} = (4 \pm 2) \times 10^{-10}$ cm^3 molecule^{-1} s^{-1} at 235 K, and no significant dependence on temperature between 235 and 222 K.

To take account of secondary chemistry, all BrO decays were fitted using a complete reaction scheme for this chemical system which is summarized in Table 4. The resulting values of k_{-1c} and the equilibrium constant K_{1c}, determined by the ratio k_{1c}/k_{-1c}, are given in Table 2.

The values of K_{1c} were used to obtain an estimate of the thermodynamic stability of Br_2O_2. Two methods were employed. In the first, a simple second law analysis of the temperature dependence of K_c between 235 and 222 K was used to determine $\Delta H^\ominus$ for reaction 1c from the Van't Hoff equation. In the second method, values of $\Delta H^\ominus$ were calculated using $\Delta G^\ominus$ from the values of K_{1c} recorded at each temperature, and the standard entropy of BrOOBr, $S^\ominus$(BrOOBr) = 327.5 J mol^{-1} K^{-1}, estimated using bond additivity[27] with $S^\ominus$(Br−O) = 147.5 J mol^{-1} K^{-1}. The results from both types of analysis are given in Table 3. As can be seen, there is excellent consistency between the values of $\Delta H^\ominus$ obtained from the temperature dependence of K_{1c} and from the individual values of K_{1c} at each temperature, giving $\Delta H^\ominus = -58.6 \pm 0.1$ kJ mol^{-1}.

TABLE 3: Thermodynamics of the Reaction BrO + BrO ⇌ Br_2O_2

T/K	K_p/atm^{-1}	$\Delta G^\ominus$/kJ mol^{-1}	$T\Delta S^\ominus$/kJ mol^{-1}	$\Delta H^\ominus$/kJ mol^{-1}
222−235				−58.65[a]
235	1.937×10^5	−23.774	−34.737	−58.51[b]
222	1.126×10^6	−25.703	−32.816	−58.52[b]

[a] From Van't Hoff analysis. [b] From third law analysis.

Although the thermodynamic analysis indicates that the values of K_{1c} may be well-determined by the data, the values of the individual rate coefficients k_{1c} and k_{-1c} may not be so well determined. The values of k_{1c} at the two temperatures give a temperature dependence expressed in T^n form of $1.05 \times 10^{-33}(T/300)^{-14.5}$ cm^6 molecule^{-2} s^{-1}. This is an excessively large negative temperature coefficient for this recombination reaction, indicating a problem with either the data or its analysis. An effect of this kind would result if the reverse decomposition of the BrOOBr molecule was not fully decoupled from its formation at short reaction times, as was assumed in the determination of k_{init}. This would lead to an underestimation of k_{init} and hence of k_{1c}, the effect being expected to diminish as temperature decreases and the lifetime of the BrOOBr molecule increases. The effect of reaction −1c on the initial decay rate would also be expected to increase with increasing pressure at a given temperature. The curvature in the plots of k_{init} vs pressure could thus be due to this effect as well as to true falloff in the recombination rate coefficient, k_{1c}. In view of the uncertainties in the data it is not possible to deduce whether the bimolecular component, k_{1b}, is pressure independent below 250 K, as assumed in the analysis. At the lowest temperature there is an indication that k_{init} at low pressure falls below the extrapolated value of k_{1b} from the pressure-

TABLE 4: Reaction Scheme Used in FACSIMILE Analysis

reaction	rate coefficient	ref	system[a]
$Br + O_3 \rightarrow BrO + O_2$	$1.7 \times 10^{-11} \exp(-800/T)^{b}$	17	I/II
$Br + BrO\ (+M) \rightarrow Br_2O\ (+M)$	$1.9 \times 10^{-14} \exp(1370/T)^{b,c}$	26	I/II
$Br + Br + M \rightarrow Br_2 + M$	$5.08 \times 10^{-34} \exp(856/T)^{d,e}$	29	I/II
$Br + Br_2O \rightarrow BrO + Br_2$	4.0×10^{-11} [b]	4	I/II
$O + O_2 + M \rightarrow O_3 + M$	$6.0 \times 10^{-32}(300/T)^{2.8}$ [e,f]	30	II
$Br_2O_2 + Br \rightarrow Br + Br_2 + O_2$	4×10^{-10} [b]	this work	I/II
$BrO + BrO \rightarrow 2Br + O_2$	$5.31 \times 10^{-12} \exp(-211/T)^{b,g}$	this work	
$BrO + BrO \rightarrow Br_{2+O2}$	$1.13 \times 10^{-14} \exp(983/T)^{b,g}$	this work	II
$BrO + BrO \rightarrow Br_2O_2$	8.2×10^{-32} [e,h]	this work	II
$Br_2O_2 \rightarrow BrO + BrO$	2.5×10^{-18} [b,h]	this work	I/II

[a] I indicates that the reaction was used in the analysis of the Br_2 photolysis experiments; II indicates that reaction was used in the analysis of the O_2 photolysis experiments. [b] Units cm^3 $molecule^{-1}$ s^{-1}. [c] This value is at atmospheric pressure (760 Torr). The reaction was assumed to be in the low-pressure limit, and this second-order rate constant was linearly extrapolated to other pressures. Note also that a value for this reaction rate coefficient was determined in this work at 235 K and 760 Torr. [d] Arrhenius expression developed from the data given in ref 29 for M = N_2. [e] Units cm^6 $molecule^{-2}$ s^{-1}. [f] Value for O_2 as bath gas. [g] Arrhenius expressions for $T > 250$ K (pressure-independent region). [h] Fitted values at 222 K.

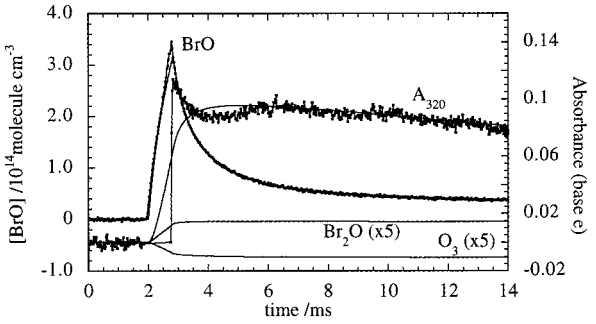

Figure 8. BrO buildup and decay trace following flashlamp photolysis of $Br_2/O_3/O_2$ mixtures at 235 K, along with the FACSIMILE fit to these data. Also shown is the temporal variation of the absorption underlying the BrO spectrum, at 320 nm (A_{320} in the figure) along with the best-fit FACSIMILE simulation of this absorption, and the contribution to this simulated absorption from Br_2O (produced) and O_3 (removed).

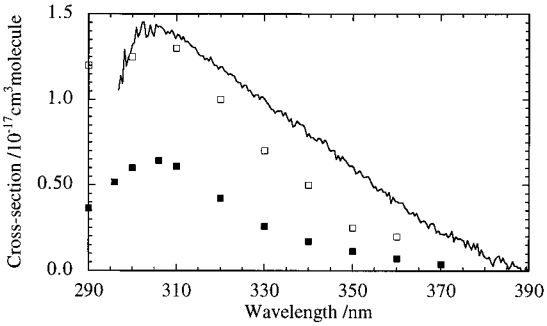

Figure 9. Absorption spectrum attributed to Br_2O_2 in this work (solid line). Also shown are the cross sections for Cl_2O_2, taken from DeMore et al.,[17] and red-shifted by 60 nm (filled squares), and the relative spectrum of the absorption attributed to Br_2O_2 by Mauldin et al.[5] (open squares).

independent region at $T > 250$ K. However, a three-parameter fit to the k_{init} data for 222 K for k_{1b}, k^0_{1c}, and k^∞_{1c} gave very large uncertainty limits for k_{1b} and k^0_{1c} (see results in parentheses in Table 2). The possibility that k_{1b} falls off as the BrOOBr formed in the pressure-dependent channel is stabilized cannot be ruled out. It is likely, therefore, that k_{1c} is significantly underestimated, especially at 235 K. However, since the determination of k_{-1c} is correlated closely to k_{1c}, the value of K_{1c} is well determined and is much less sensitive to the absolute individual values of k_{1c} and k_{-1c}.

The full reaction scheme for the low-temperature BrO self-reaction system in ozone was also used to simulate the temporal behavior of the absorption underlying the BrO spectra as well as the BrO decay. Figure 8 shows a BrO decay from an experiment at 235 K, along with the experimental underlying absorption at 320 nm. The FACSIMILE simulation of this BrO decay is also shown, along with the best fit simulated absorption at 320 nm, incorporating the contributions from Br_2O and O_3 and optimizing the cross section of Br_2O_2 at this wavelength Although the quality of the fit at short times after the flash is rather poor, which is attributed to the effect of scattered flashlamp intensity, the level of absorbance reached is well reproduced by the simulation. The best fit to the data was obtained with a Br_2O_2 cross section of 1.2×10^{-17} cm^2 $molecule^{-1}$ at 320 nm. Figure 9 shows the spectrum assigned to Br_2O_2 (after the subtraction of the contributions of O_3 and Br_2O) scaled to this cross section value at 320 nm. The shape of the spectrum observed by Mauldin et al.[5] is also shown, and the spectrum of Cl_2O_2, taken from DeMore et al.[17] and red-shifted by 60 nm, is also shown for comparison. The value of the cross section at the maximum is approximately a factor of 2 higher than the value for the dimer of ClO, which is reasonable considering the trends of absorption characteristics for other halogen species.

Photolysis of O_2 in the Presence of Br_2. The 193 nm photolysis of O_2 produces atomic oxygen in the (^3P) electronic state through absorption in the Schumann−Runge bands and the underlying Hertzberg continuum. In this system the oxygen atoms can react with either Br_2 or O_2 to produce BrO or O_3, respectively:

$$O(^3P) + Br_2 \rightarrow BrO + Br \quad (5)$$

$$O(^3P) + O_2 + M \rightarrow O_3 + M \quad (13)$$

The relative concentrations of BrO and O_3 produced are therefore determined by the relative values of ($k_5[Br_2]$) and ($k_{13}[O_2][M]$). Ideally, the $[Br_2]$ should be kept sufficiently high to ensure stoichiometric conversion of O atoms to BrO, but as Br_2 has a significant absorption at 193 nm ($\sigma \approx 2 \times 10^{-20}$ cm^2 $molecule^{-1}$), the experimental concentrations of Br_2 were restricted by the need to keep the optical depth of the cell low enough to preclude longitudinal concentration gradients of BrO. Furthermore, oxygen concentrations were necessarily high to ensure that sufficient oxygen atoms were produced. Thus, some ozone was inevitably formed in these experiments.

The concentrations of O_3 and BrO were determined by spectral fitting as described above. However, photolysis of atmospheric oxygen by the laser in the analysis beam light path external to the cell produced some ozone, and therefore, the observed ozone absorption could not be related directly to the

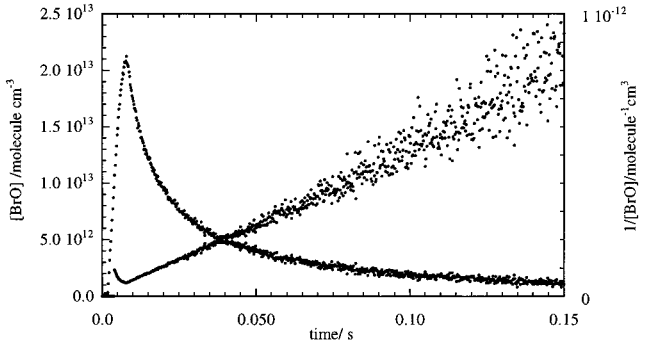

Figure 10. BrO buildup and decay following laser photolysis of O_2/Br_2 mixtures at 298 K. Also shown is the corresponding second-order plot (1/[BrO] vs time) for these data.

quantity of ozone formed within the cell. Two methods were used to determine the concentration of ozone within the cell. An estimate of the concentration of ozone produced outside the cell was gained by performing flash photolysis experiments with an evacuated cell, and the measured ozone concentration (attributed to extracellular ozone) was subtracted from that determined in the actual BrO experiments. A more rigorous measurement was achieved by performing flash experiments at a range of reaction vessel pressures. Since ≫99% of the reaction vessel pressure consisted of oxygen, at low pressures $k_5[Br_2] \gg k_{13}[O_2][M]$ and the initial BrO concentration ($[BrO]_0$) is equated to the quantity of photochemically produced O atoms ($[O]_0$). Thus, knowing that the laser output power was constant (to within about 5% rms) and ensuring that the reaction mixture was optically thin (i.e., absorbance < 0.4) at 193 nm, the value of $[O]_0$ was assumed to increase linearly with O_2 pressure and was therefore extrapolated to higher pressures. For a given set of experimental conditions, it was found that the initial BrO concentration varied linearly with pressure at low pressures but fell off at higher pressures. The quantity of ozone produced in the cell was then simply determined from the expression ($[O_3] = [O]_0$(extrapolated) − $[BrO]_0$).

Experiments were performed at a range of pressures between 100 and 760 Torr and at temperatures of 298, 267, 250, 235, and 222 K. The decay of BrO radicals was found to be second order under all conditions. The presence of the BrO dimer (Br_2O_2) was not expected to affect the second-order kinetics since the excess of Br atoms, generated concurrently with the BrO radicals from reaction 5 and subsequently in reaction 1a, ensured that any dimer formed was rapidly consumed in reactions 12 and −10. The measured BrO decay therefore resulted from all channels of the self-reaction. Hence

$$-\mathrm{d[BrO]}/\mathrm{d}t = 2(k_{1a} + k_{1b} + k_{1c}[M])[BrO]^2 \qquad \text{(iv)}$$

A typical BrO decay and second-order plot are shown in Figure 10. At low pressures, where $k_5[Br_2] \gg k_{13}[O_2][M]$ and the amount of ozone formed in the cell was negligible, the slopes of the second-order plots gave the value of $2(k_{1a} + k_{1b} + k_{1c}[M])$. At higher pressures the small quantities of photochemically produced ozone ($(1-10) \times 10^{12}$ molecules cm^{-3}) led to some regeneration of BrO through reaction 2 and a partial masking of channel 1a. Thus, FACSIMILE was used to analyze these decay traces. The quantity of BrO regeneration was determined by the ozone concentration (measured) and the number of Br atoms removed in processes other than the reaction of Br with ozone (i.e., reactions 7, 8, and 9). All of the rate constants used in this analysis are given in Table 4. In the simulation, the values of the rate coefficients for the bimolecular and termolecular channels of the BrO self-reaction 1b and 1c were set at the values determined from k_{init} in the Br_2 photolysis experiments: $[BrO]_0$ and k_{1a} were then varied to optimize the fit to the decay traces.

TABLE 5: Rate Coefficients for the BrO + BrO Reaction as a Function of Temperature and Pressure

T/K	press./ Torr	k_{1a}[a]/10^{-12} cm^3 molecule^{-1} s^{-1}	$k_{1b} + k_{1c}$[M][b]/10^{-12} cm^3 molecule^{-1} s^{-1}	k_1[c]/10^{-12} cm^3 molecule^{-1} s^{-1}
298	100−760	2.59 ± 0.28	0.31 ± 0.02	2.90 ± 0.28
267	100−760	2.46 ± 0.46	0.43 ± 0.01	2.89 ± 0.46
250	100−760	2.25 ± 0.29	0.59 ± 0.03	2.84 ± 0.29
235	103	1.51 ± 0.21	0.83 ± 0.06	2.34 ± 0.22
	104	1.76 ± 0.25	0.84 ± 0.06	2.60 ± 0.26
	184	1.39 ± 0.21	0.95 ± 0.10	2.34 ± 0.23
	204	1.68 ± 0.09	0.98 ± 0.11	2.66 ± 0.14
	205	1.50 ± 0.11	0.98 ± 0.11	2.48 ± 0.16
	375	1.62 ± 0.17	1.24 ± 0.19	2.86 ± 0.25
	407	1.52 ± 0.31	1.28 ± 0.20	2.80 ± 0.37
	543	1.48 ± 0.22	1.49 ± 0.27	2.97 ± 0.35
	566	1.59 ± 0.22	1.52 ± 0.28	3.11 ± 0.36
	760	1.66 ± 0.14	1.81 ± 0.38	3.47 ± 0.40
	778	1.60 ± 0.23	1.83 ± 0.39	3.43 ± 0.45
222	106	0.59 ± 0.18	1.21 ± 0.23	1.80 ± 0.26
	203	0.40 ± 0.06	1.55 ± 0.24	1.95 ± 0.24
	411	0.52 ± 0.16	2.30 ± 0.30	2.82 ± 0.33
	560	0.55 ± 0.14	2.83 ± 0.35	3.38 ± 0.37
	778	0.35 ± 0.10	3.61 ± 0.43	3.96 ± 0.44

[a] For $T \geq 250$ K, k_{1a} given is the mean of all values obtained at pressures 100−760 Torr. For $T < 250$, k_{1a} is given from the FACSIMILE fit to each trace at the pressure indicated. All errors are 1σ. [b] Parametrized value of k_{init} from the Br_2 photolysis experiments. [c] $k_1 = (k_{1a} + k_{1b} + k_{1c}[M])$.

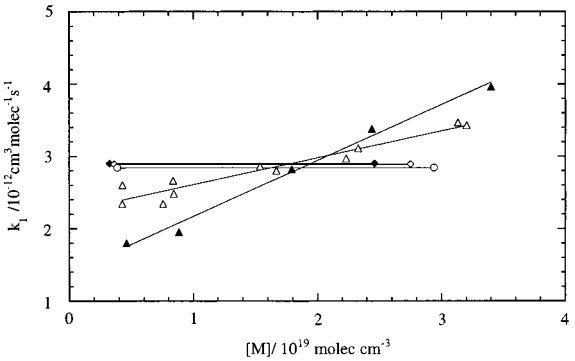

Figure 11. Overall rate coefficient, k_1, for the BrO self-reaction plotted as a function of pressure for all temperatures studied in this work. For clarity, the pressure-independent average values of k_1 are given at $T \geq 250$ K, linked by symbols. Legend: filled triangles, 222 K; open triangles, 235 K; open circles, 250 K; open diamonds, 267 K; filled diamonds, 298K.

Table 5 and Figure 11 show the total rate coefficients for the overall BrO self-reaction (k_1) as a function of pressure for all temperatures studied. Virtually no pressure dependence to k_1 is observed between 760 Torr and about 100 Torr at $T > 250$ K. Average values of k_1 and k_{1a} are given for these temperatures. Above 250 K, k_{1a} is adequately described by the Arrhenius expression $k_{1a} = (5.31 \pm 1.17) \times 10^{-12} \exp[(211 \pm 59)/T]$ cm^3 molecule^{-1} s^{-1}. At 235 and 222 K the overall rate coefficient is pressure dependent, increasing with decreasing temperature at high pressure, but decreasing significantly with decreasing temperature at low pressure. These results are also shown in Figure 13 and are discussed below.

In addition to the rate parameters determined for the BrO self-reaction in these experiments, the measurement of the relative concentrations of BrO and O_3 produced following the photolysis of O_2 in this system enabled the rate coefficient of

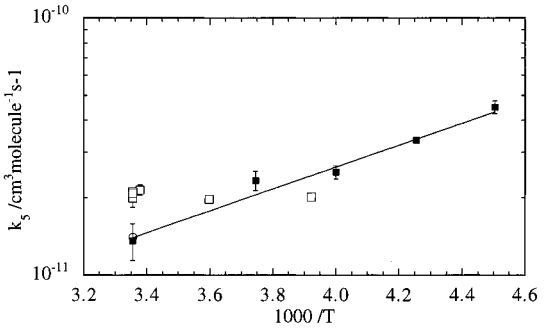

Figure 12. Rate coefficient, k_5, of the O + Br_2 reaction plotted as a function of (1000/*T*) (filled squares), along with an Arrhenius fit to these data. Also shown are the results of Nicovich and Wine[31] (open squares), and the recommendation of Atkinson et al.[30] (open circle).

reaction 5 to be determined relative to the rate coefficient of reaction 13. Assuming that the photochemically produced O atoms react only with O_2 and Br_2 in this system, then

$$\frac{[BrO]_0}{[O_3]_0} = \frac{k_5[Br_2]}{k_{13}[O_2][M]}$$

$[BrO]_0$, $[O_3]_0$, and $[Br_2]$ were measured and k_{13} was taken from Atkinson et al.[30] The values for k_5 determined in this way are given in Table 6 and are shown in Arrhenius form in Figure 12 with previous measurements of this rate constant[31] for comparison. These data are fitted by the Arrhenius expression $k_5 = (5.12 \pm 1.86) \times 10^{-13} \exp[(989 \pm 91/T)]$ cm^3 molecule^{-1} s^{-1}.

Errors

All errors reported in this work and quoted in Tables 2 and 5 are given at the 1σ level and represent statistical uncertainty from repeated measurements only. They give no indication of the potential systematic errors in determination of rate parameters. A significant systematic error in this work is the uncertainty in the BrO cross sections used to determine BrO concentrations. The cross sections used in this work, from Wahner et al.,[21] are uncertain to ±10%. More recent measurements seem to favor the lower end of this range.[28] We estimate an additional error of 5−10% in the rate constants for the individual channels at temperatures ≥250 K, but larger errors in the data at lower temperatures, principally because of the uncertainty arising from the assumptions concerning the partitioning between the different reaction channels. In particular, the values of k_{1a} reported here will have additional uncertainty since k_{1a} is effectively determined from the difference in the BrO decay rates in the presence and absence of ozone.

Discussion

Comparison with Previous Studies. The kinetic parameters for the BrO self-reaction obtained in the present work are compared with previous measurements in Figure 13a−c. In Figure 13a, previous measurements of the overall rate constant (k_1) are shown as a function of temperature. On the plot, vertical lines between points indicate that pressure-dependent measurements have been made. There is excellent agreement between the value of k_1 determined in this study and previous measurements at room temperature, where no pressure dependence has been found. At 250 K, k_1 reported here is in close agreement

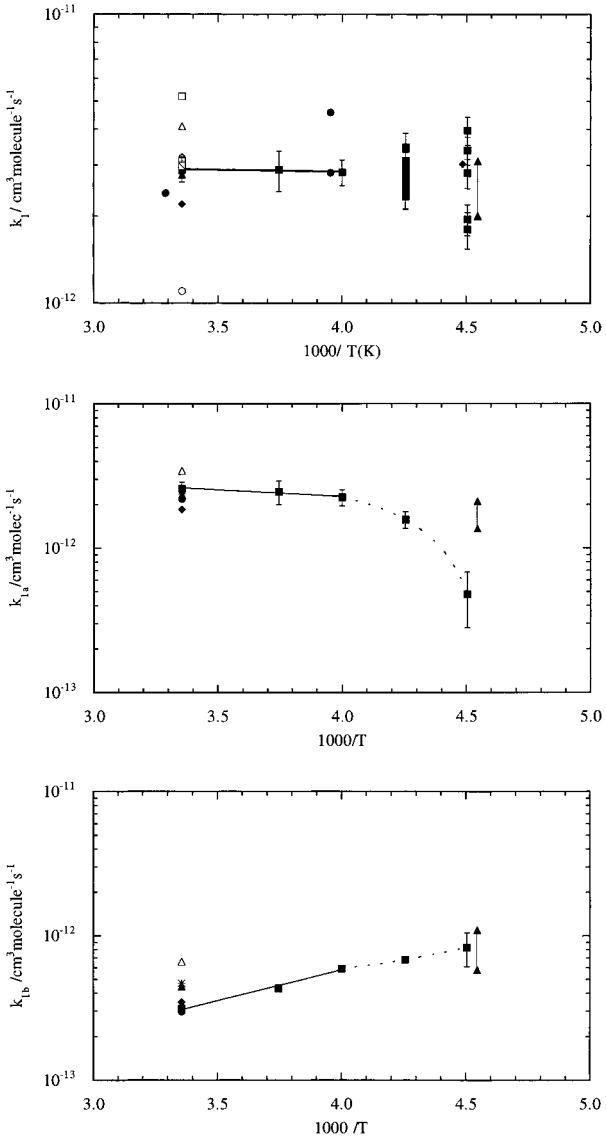

Figure 13. Comparison of previous measurements of *k*(BrO+BrO) with this study: (a) k_1, (b) k_{1a}, (c) k_{1b}: filled squares, this work; open squares, Clyne and Cruse;[7] open circles, Basco and Dogra;[8] open diamonds, Clyne and Watson;[9] filled diamonds, Sander and Watson;[6] open triangles, Cox et al.;[11] filled circles, Turnipseed et al.;[12] vertical crosses (+): Lançar et al.;[13] filled triangles: Mauldin et al.;[5] crossed boxes: Bridier et al.;[14] crosses (x): Rowley et al.;[4] horizontal lines: Laszlo et al.[16] For clarity, error bars are shown for this work only. The data of Mauldin et al. at low temperature are shown only at the extremes of pressure, connected by a vertical line.

TABLE 6: Rate Coefficient for O + Br_2 Reaction, k_5, at 760 Torr as a Function of Temperature

T/K	k_5[a]/10^{-11} cm^3 molecule^{-1} s^{-1}	*T*/K	k_5[a]/10^{-11} cm^3 molecule^{-1} s^{-1}
298	1.36 ± 0.3	235	3.35 ± 0.3
267	2.33 ± 0.2	222	4.50 ± 0.4
250	2.51 ± 0.2		

[a] Errors are 1 σ.

with the lower of the two values reported by Turnipseed et al.[12] at 253 K and 2 Torr. At lower temperatures, the pressure-dependent values of k_1 obtained in this study (100−760 Torr, M = N_2) encompass those of Mauldin et al.[5] (75−600 Torr, M = He, N_2, and SF_6) and Sander and Watson[6] (50−475 Torr, M = He). The values of Mauldin et al.[5] were obtained indirectly from their measurements of k_{1b} and the branching ratio, α (α

$= k_{1a}/k_1$). The magnitude of the pressure dependence for k_1 reported here at 222 K is greater than that reported by Mauldin et al.[5] at 220 K and by Sander and Watson,[6] who observed only a 20% reduction in k_1 at the lowest pressure used (50 Torr of He) at 223 K and report a pressure-independent value of k_1. Below 250 K the overall rate coefficient becomes pressure dependent and shows a small increase with decreasing temperature at the highest pressure used (760 Torr), but at low pressure, k_1 falls off with decreasing temperature.

Figure 13b shows previous measurements of the rate constant for channel 1a (k_{1a}) of the BrO self-reaction in comparison with this work. At 298 K, there is excellent agreement between the value of k_{1a} reported here and previous studies, which have either determined k_{1a} directly from measurements of k_1 and k_{1b} or inferred k_{1a} from measurements of k_1 and the branching ratio, α. At lower temperatures, the value of k_{1a} determined here at 222 K is much smaller than that calculated from the work of Mauldin et al., who measured k_{1b} and α at 220 K. However, for the reasons discussed below we believe they may have overestimated k_{1b} and hence k_{1a}.

Figure 13c shows previous measurements for the rate constant for channel 1b of the BrO + BrO reaction, compared with k_{1b} determined in this work. As with the other bimolecular channel 1a, k_{1b} determined here is in good agreement with previous studies at ambient temperature. At temperatures above 250 K, k_{1b} is independent of pressure from 100 to 760 Torr and shows a small negative activation energy of 8.2 kJ mol^{-1}, typical of a radical + radical reaction proceeding through a short-lived intermediate. Below 250 K, k_{1b} is not well-defined in our work. We observe a pressure dependence in the overall rate constant, k_1, which is attributed to the formation of a stabilized BrOOBr dimer in the termolecular channel 1c, which appears to compete with one or both of the bimolecular channels. Assuming that k_{1b} is independent of pressure, our values of k_{1b} at 222 K agree well with those reported by Mauldin et al., at 220 K and intermediate pressure (200 Torr). Mauldin et al. also observed a pressure dependence of the BrO + BrO reaction at low temperature, which they attributed to the molecular channel 1b. The overall rate coefficient, k_1, deduced from their value of k_{1b} at 220 K is in good agreement with that measured in the present work at 222 K but did not show the departure from second-order kinetic behavior which was observed in the present work. In both studies BrO was monitored by differential spectroscopy, so interfering absorption by BrO dimer is not the explanation of this discrepancy. Mauldin et al. observed a transient absorption spectrum at 220 K which was assigned to the dimer, BrOOBr, and they attributed the departure from second order observed when BrO was monitored at a single wavelength to absorption by the dimer. The most likely explanation for the apparent enhancement of the second-order rate coefficient at higher pressures observed by Mauldin et al. is scavenging of the BrO dimer by reaction with Br, reaction 12. Based on observations in the present work, the relatively low $[O_3]$ used by Mauldin et al. in their diode array experiments would have been insufficient to reduce [Br] to a level where scavenging of the dimer in reaction 12 was not significant.

As shown in Figure 8, inclusion of the reversible channel 1c in the reaction scheme for modeling this system allows the temporal behavior of the BrO and the absorption attributed to the BrO dimer, Br_2O_2, to be reproduced in our experiments. Thus, at least part of the observed pressure dependence in k_1 in the initial stages is due to channel 1c. Our results do not allow an unequivocal conclusion to be drawn concerning the effect of pressure on k_{1a} or k_{1b} at low temperature. However, we believe that the rate coefficients assigned by Mauldin et al. to reaction 1b at high pressures are too high and include some contribution from the channel forming the dimer.

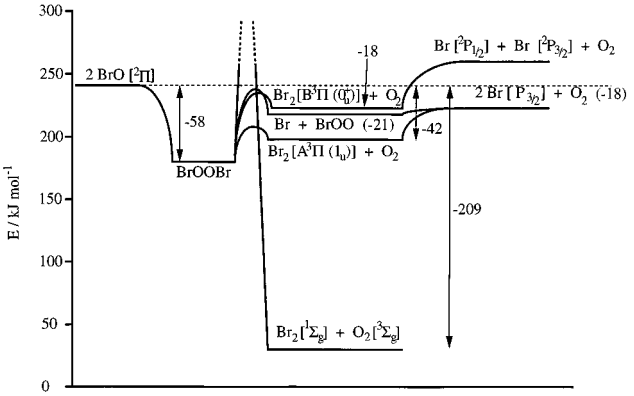

Figure 14. Schematic representation of the potential energy of BrO, intermediates and products in the BrO + BrO reaction.

In summary, although the overall rate constant for the BrO self-reaction shows little temperature dependence, the partitioning of k_1 between channels changes significantly with temperature. Above 250 K channels 1a and 1b show Arrhenius behavior with zero and negative temperature dependence, respectively, and with no pressure dependence. At lower temperatures both channel 1a and channel 1b show a falloff in the rate constant from the extrapolated higher temperature results. This is accompanied by the emergence of a reversible pressure-dependent termolecular channel 1c, forming a dimer, making the overall rate constant pressure dependent. These results are discussed in mechanistic terms below.

Mechanism. The reaction mechanism for the BrO self-reaction is based upon the scheme originally proposed by Porter[32] for the ClO self-reaction, involving, in this case, the excited BrOOBr* intermediate:

$$BrO + BrO \rightleftharpoons BrOOBr^* \rightarrow \text{products}$$

The energy diagram for the formation of intermediates and products, constructed using the most up to date enthalpy data, is shown in Figure 14. The chemically activated intermediate formed from two BrO radicals can decompose unimolecularly or undergo collisional stabilization. Channel 1a, forming atomic products, could result from the decomposition of BrOOBr* by simple cleavage of the Br−O bond:

$$BrOOBr^* \rightarrow Br + BrOO$$

Subsequent rapid decomposition of the unstable BrOO species leads to formation of a second Br atom:

$$BrOO \rightarrow Br + O_2$$

As discussed above, BrOO has never been observed, and all evidence points to it being unstable (D(Br−OO) $\approx$ 4 kJ mol^{-1} [5,33]).

k_{1a} has no pressure dependence, indicating that the lifetime of the BrOOBr* is too short for collisional deactivation to be effective or that the deactivated product also dissociates rapidly to give Br + BrOO. This channel also shows no significant temperature dependence above 250 K, so the activation barrier for Br−O cleavage must lie close to or below the energy of

BrO reactants. The reverse reaction of Br with BrOO radicals is also likely to have near zero activation energy.

k_{1b} is also pressure independent above 250 K and exhibits a small negative temperature dependence, suggesting a bimolecular reaction proceeding through a complex. A four-center transition state is usually invoked for the concerted elimination of molecular products:

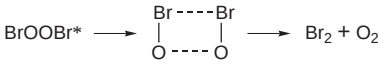

The mechanism for this "molecular channel" in the self- and cross-reactions of halogen oxides has been discussed in detail by Toohey and Anderson,[34] in the context of their results for BrCl formation in the ClO + BrO reaction. They argue that electronically excited $BrCl(^3\Pi_{0+})$ is formed together with ground-state $O_2(^3\Sigma_g^-)$ by four-center elimination from an internally excited singlet BrOOCl molecule. The $BrCl(^3\Pi_{0+})$ can be formed with vibrational excitation and is subsequently quenched or fluoresces, forming ground-state $BrCl(^1\Sigma_g^-)$, or predissociates, giving Br and Cl atoms in the $^2P_{3/2}$ ground state. In the case of the BrO + BrO reaction, formation by molecular elimination of both the lowest $A(^3\Pi_{1u})$ and the $B(^3\Pi_{0u}^+)$ states of Br_2 is energetically allowed (Figure 14), and emission from both states has been observed from low-pressure systems containing BrO.[7] Since the reaction has a negative temperature dependence, the activation barrier for the four-center reaction must also be below the level of the BrO reactants. A low activation barrier for the four-center process forming electronically excited products can be qualitatively rationalized in terms of the orbital symmetry constraints embodied in the Woodward−Hoffmann rules,[35] which predict that for reactions involving cyclic intermediates formation of ground-state products can only occur with high activation energy, while formation of excited triplet products can be formed with a low barrier. Above 250 K, collisional stabilization of BrOOBr* does not intercept the formation of molecular products through the four-centered transition state, and no pressure dependence results.

Below 250 K, the observed pressure dependence of the second-order rate coefficient for BrO decay in the initial stages of the reaction, under conditions where the BrOOBr molecule is not scavenged by Br atoms, is consistent with collisional quenching of the chemically activated BrOOBr* complex to form the thermally equilibrated dimer, BrOOBr. The overall rate coefficient for BrO loss at high pressure is only slightly increased at 222 K, suggesting that at lower temperatures collisional deactivation competes against the unimolecular decomposition of the initially formed complex. Decomposition of the thermalized BrOOBr can then occur by collisional activation to a thermally activated BrOOBr* molecule which decomposes unimolecularly to produce atomic and molecular products in channels 1a or 1b or to produce two BrO radicals in the reverse reaction −1c. In the present experiments an absorption attributed to BrOOBr is observed, and the temporal variation of this absorption can be modeled, along with the observed non-second-order BrO kinetics, using a reaction scheme incorporating this reversible formation of BrOOBr from BrO at low temperatures (Figure 8). This implies that under these conditions the decomposition of BrOOBr* to BrO dominates over product formation. Thus, the overall rates of formation of products Br and Br_2 depend on the relative rates of the unimolecular processes, which depend, in turn, on the degree of excitation of the BrOOBr.

The mechanism proposed for the BrO + BrO reaction at low temperatures is summarized as follows:

$$\mathrm{BrO} + \mathrm{BrO} \rightleftharpoons \mathrm{BrOOBr}^* \qquad k_c, k_{-c}$$

$$\mathrm{BrOOBr}^* + \mathrm{M} \rightleftharpoons \mathrm{BrOOBr} + \mathrm{M} \qquad k_q, k_{-q}$$

$$\mathrm{BrOOBr}^* \rightarrow \mathrm{Br} + \mathrm{BrOO} \qquad k_a$$

$$\mathrm{BrOOBr}^* \rightarrow \mathrm{Br}_2 + \mathrm{O}_2 \qquad k_b$$

Assuming steady state for BrOOBr*, the rate of loss of BrO is given by

$$-\frac{1}{2}\frac{d[BrO]}{dt} = k_c[BrO]^2 - \frac{k_{-c}(k_c[BrO]^2 + k_{-q}[BrOOBr][M])}{k_{-c} + k_a + k_b + k_q[M]} \quad (v)$$

Under conditions where the reverse decomposition of BrOOBr is unimportant, i.e., in the initial stages after BrO production or when it is removed by reaction with Br, the overall rate coefficient takes the form

$$-\frac{1}{2}\frac{d[BrO]}{dt} = \frac{k_c(k_q[M] + k_a + k_b)}{k_{-c} + k_a + k_b + k_q[M]}[BrO]^2 \quad (vi)$$

The magnitude of the pressure dependence of the overall rate constant will depend on the relative magnitudes of the unimolecular steps. A larger pressure dependence for the overall loss of BrO is expected under the conditions of excess O_3, when the Br-forming channel leads to regeneration of BrO, and k_a is effectively removed from the above expression.

In our experiments under these conditions, formation of the thermally equilibrated dimer from BrO appeared to be reversible, implying that $k_{-c} \gg k_b$. In the later stages of the reaction BrOOBr is in steady state, and its formation only acts as a reservoir and does not lead to overall loss of BrO. (Under typical experimental conditions, BrOOBr was observed to equilibrate with BrO over time scales of 8−12 ms at 235 K and 5−8 ms at 222 K.) Under these conditions the rate equation takes the simpler form

$$-\frac{1}{2}\frac{d[BrO]}{dt} = \frac{k_c(k_a + k_b)}{k_{-c} + k_a + k_b}[BrO]^2 \quad (vii)$$

and the overall rate coefficients for the two bimolecular channels can be expressed as

$$k_{1a} = \frac{k_c k_a}{k_{-c} + k_a + k_b} \quad (viii)$$

$$k_{1b} = \frac{k_c k_b}{k_{-c} + k_a + k_b} \quad (ix)$$

These expressions will also apply for the higher temperatures where the chemically activated complex of higher energy is formed.

While this mechanism does explain the change in partitioning between the bimolecular and termolecular channels of the BrO self-reaction and does rationalize the increase in k_1 at low temperature and high pressure, the reason for the observed falloff in k_1 at low temperature and low pressure is not clear. Under these conditions, the collisional quenching of BrOOBr* would

not compete as effectively with the unimolecular decomposition of this complex, and k_1 should not be significantly reduced. Thus, we are unable to completely explain the apparent falloff in k_1 under these conditions.

Information on the relative rates of the two bimolecular channels has been obtained previously from measurements of the chain length for ozone loss in the presence of BrO, which gives the branching ratio $\alpha = k_{1a}/k_1$. At the temperatures used in previous studies of this reaction, the formation of BrOOBr is reversible and does not lead to permanent removal of BrO. Consequently, the overall quantum yield for ozone removal is still determined only by the relative rates of the channels 1a and 1b. Mauldin et al.[5] measured a value of $\alpha = 0.68$ at 220 K which was independent of pressure, while at the same time k_{1b} was pressure dependent. This can be understood in terms of the mechanism proposed here if the activation barriers for the unimolecular processes k_a and k_b are approximately equal. The relative rates of the two product forming channels are then determined largely by their *A* factors; the values for Br−OOBr cleavage is likely to be $\sim 10^{14.0}$ s^{-1} and for the four-center elimination of Br_2, $\sim 10^{13.0}$ s^{-1}, which is consistent with the observed overall product yields. Finally, the absence of any OBrO product in reaction 1 suggests that the BrOBrO complex, if formed, has a high-energy barrier to cross in cleaving the terminal Br−OBrO bond.

The mechanism for the BrO + BrO reaction is analogous in many respects to the ClO + ClO reaction (ref 17 and references therein). However, the stability of the BrOOBr dimer relative to 2BrO is much lower than ClOOCl relative to 2ClO: ΔH_r (BrOOBr) = −58.6 kJ mol^{-1} obtained here, compared to ΔH_r (ClOOCl) = −73.5 kJ mol^{-1}.[17] Consequently, the formation of significant amounts of the stabilized BrOOBr complex in the termolecular reaction channel only occurs at much lower temperatures than stabilized ClOOCl formation in the ClO self-reaction. Furthermore, since the bimolecular channels in the ClO self-reaction all have a significant positive activation energy, the reactions are relatively slow and only become significant compared to dimer formation at temperatures above $T \approx 273$ K. The bimolecular channels of BrO dominate even at low temperatures.

Atmospheric Implications. Although the BrO radical is important in the stratosphere, the BrO self-reaction is of very minor significance because of the low mixing ratio of BrO in this region. The main reactions of BrO leading to ozone loss are those involving ClO and HO_2. The formation of Br_2O_2 as a product of reaction 1 is unlikely to alter this conclusion. Br_2O_2 is unlikely to form in the stratosphere owing to the low pressure in this region. Moreover, Br_2O_2 is so unstable with respect to reverse decomposition to BrO + BrO that the stratospheric lifetime of Br_2O_2 would be very short. Consequently, the photolysis of Br_2O_2 to yield Br and BrOO would not contribute significantly to stratospheric ozone depletion in a cycle analogous to that involving Cl_2O_2.

In the troposphere, specifically the polar marine boundary layer in springtime, the abundance of BrO can be high enough for reaction 1 to take place. However, the temperature in this region of the atmosphere would not be low enough for the Br_2O_2 species to form, and the Arrhenius expressions for k_{1a} and k_{1b}, fitted at temperatures ≥250 K, are appropriate for atmospheric models of tropospheric bromine chemistry.

Conclusions

This study of the kinetics of the self-reaction of BrO radicals has provided rate data over an extended range of conditions which give new insight into the mechanism for the reaction. The rate constants at $T > 250$ K are in excellent agreement with earlier measurements made by a variety of techniques. It has shown from experiments at lower temperature that the reaction has a third termolecular channel which forms the BrO dimer. The spectrum attributed to the BrO dimer has been recorded and has a similar shape to that of the ClO dimer with a peak at about 305 nm with a cross section of 1.4×10^{-17}cm^2 molecule^{-1} (1.2×10^{-17} cm^2 molecule^{-1} at 320 nm). No evidence for any channel giving OBrO was observed. The reaction mechanism involves the formation of an energy-rich BrOOBr association complex, which decomposes unimolecularly into products. At low temperatures this complex can be quenched by collisions to form a weakly bound dimer, which decomposes preferentially back to reactants. Similar mechanisms probably operate in all XO + XO reactions, (X = Cl, Br, and I), which have been found to exhibit a richly complex kinetic behavior.

In addition to the rate constants determined for the BrO self-reaction, this study has provided new measurements of the rate parameters for the reaction between O + Br_2 ($k_5 = (5.12 \pm 1.86) \times 10^{-13} \exp[(989 \pm 91/T)]$ cm^3 molecule^{-1} s^{-1}). The negative temperature dependence for an apparently simple abstraction reaction is perhaps surprising, although there is increasing evidence for complex formation in reactions of an electronegative atom with highly polarizable Br and I atoms in a molecule.[36] Rate coefficients were also determined for the termolecular reaction between Br and BrO ($k_7 = (9.1 \pm 2.0) \times 10^{-12}$ cm^3 molecule^{-1} s^{-1} at 235 K, 760 Torr) and for the reaction between Br and Br_2O_2 ($k_{12} = (4 \pm 2) \times 10^{-10}$ cm^3 molecule^{-1} s^{-1} , 222−235 K).

Acknowledgment. The authors would like to thank the UK NERC (Contract GST/02/1046) and the EC (Contract EV5V CT 93 0338, "CABRIS" project) for funding this project. M.H.H. thanks NERC for the award of a studentship. D.R. thanks NERC for the award of an advanced fellowship. The authors thank Professor B. A. Thrush for helpful discussions.

References and Notes

(1) WMO Global Ozone Research and Monitoring Project, Report No. 37, Scientific Assessment of Ozone Depletion, 1994; World Meteorological Organisation, Geneva, 1994.
(2) Barrie, L. A.; Bottenheim, J. W.; Hart, W. R. *J. Geophys. Res.* **1994**, *12, 25,313.*
(3) Hausmann, M.; Platt, U. *J. Geophys. Res.* **1994**, *12, 25, 399.*
(4) Rowley, D. M.; Harwood, M. H.; Freshwater, R. A.; Jones, R. L. *J. Phys. Chem.* **1996**, *100*, 3020.
(5) Mauldin, R. L. III; Wahner, A.; Ravishankara, A. R. *J. Phys. Chem.* **1993**, *97*, 7585.
(6) Sander, S. P.; Watson, R. T. *J. Phys. Chem.* **1981**, *85*, 4000.
(7) Clyne, M. A. A.; Cruse, H. W. *Trans. Faraday Soc.* **1970**, *66,* 2214.
(8) Basco, N.; Dogra, S. K. *Proc. Roy. Soc. London, Ser. A* **1971**, *323*, 417.
(9) Clyne, M. A. A.; Watson, R. T. *J. Chem. Soc., Faraday Trans. 1* **1975**, *71*, 336.
(10) Jaffe, S.; Mainquist, W. K. *J. Phys. Chem.* **1980**, *84*, 3277.
(11) Cox, R. A.; Sheppard, D. W.; Stevens, M. P. *J. Photochem.* **1982**, *19*, 189.
(12) Turnipseed, A. A.; Birks, J. W.; Calvert, J. W. *J. Phys. Chem.* **1990**, *94*, 7477.
(13) Lançar, I. T.; Laverdet, G.; LeBras, G.; Poulet, G. *Int. J. Chem. Kinet.* **1991**, *23*, 37.
(14) Bridier, I.; Veyret, B.; Lesclaux, R. *Chem. Phys. Lett.* **1993**, *201*, 563.
(15) Rattigan, O. V.; Cox, R. A.; Jones, R. L. *J. Chem. Soc., Faraday Trans.* **1995**, *91*, 4189.
(16) Lazlo, B.; Kurylo, M. J.; Huie, R. E. *J. Phys. Chem.* **1995,** *99,* 11701.
(17) DeMore, W. B.; Sander, S. P.; Golden, D. M.; Hampson, R. F.; Kurylo, M. J.; Howard C. J.; Ravishankara, A. R.; Kolb, C. E.; Molina, M.

J. Chemical Kinetics and Photochemical Data for Use in Stratospheric Modeling, JPL publication 97-4, California Institute of Technology, Pasadena, 1997.

(18) Nickolaisen, S. L.; Friedl, R. R.; Sander, S. P. *J. Phys. Chem.* **1994**, *98*, 155.

(19) Harwood, M. H.; Jones, R. L. *J. Geophys. Res.* **1994**, *99*, 22955.

(20) Harwood, M. H. Ph.D. Dissertation, University of Cambridge, 1995.

(21) Wahner, A.; Ravishankara, A. R.; Sander, S. P.; Friedl, R. R. *Chem. Phys. Lett.* **1988**, *152*, 507.

(22) Daumont, D.; Brion, J.; Charbonnier, J.; Malicet, J. *J. Atmos. Chem.* **1992**, *15*, 145.

(23) Seery, D. J.; Britton, D. *J. Phys. Chem.* **1964**, *68*, 2263.

(24) Rattigan, O. V.; Lary, D. J.; Jones, R. L.; Cox, R. A. *J. Geophys. Res*. **1995,** *101*, 23021.

(25) Curtis, A. R.; Sweetenham, W. P. FACSIMILE, AERE Harwell publication R 12805, Computer Science and Systems Division, Harwell Laboratory, Oxfordshire, U.K., 1987.

(26) Hayman, G. D.; Danis, F.; Thomas, D. A. In Proceedings of Air Pollution Research Report 45: "Chemical Mechanisms Describing Tropospheric Processes"; Peeters, J., Ed.; CEC Publications, Leuven, Belgium, 1992.

(27) Benson, S. W. *Thermochemical Kinetics*, 2nd ed.; John Wiley and Sons: New York, 1976.

(28) Burkholder, J. B. Presented at the 14th International Symposium on Gas Kinetics, Leeds, U.K., 1996.

(29) National Institute for Standards and Technology, Chemical Kinetics Database, distributed by NIST Standard Reference Data, Gaithersburg, MD 20899.

(30) Atkinson, R.; Baulch, D. L.; Cox, R. A.; Hampson, R. F.; Kerr, J. A.; Troe, J. Evaluated Kinetic and Photochemical Data for Atmospheric Chemistry−Supplement IV, IUPAC Subcommittee on Gas Kinetic Data Evaluation for Atmospheric Chemistry. *J. Phys. Chem. Ref. Data* **1992**, *21*, 1125.

(31) Nicovich, J. M.; Wine, P. H. *Int. J. Chem. Kinet.* **1990**, *22*, 379.

(32) Porter, G. *Proc. R. Soc. London, A* **1950**, *200*, 284.

(33) Brown, J.; Burns, G. *Can. J. Chem.* **1970**, *48*, 3487

(34) Toohey, D. W.; Anderson, J. G. *J. Phys. Chem.*, **1988**, *92*, 1705.

(35) Woodward, R. B.; Hoffman, R. *Angew. Chem., Int.* Ed. *Engl*. **1969**, *8*, 781.

(36) Bilde, M.; Sehested, J.; Nielsen, O. J.; Wallington, T. J.; Meagher, R. J.; McIntosh, M. E.; Piety, C. A.; Nicovich, J. M.; Wine, P. H. *J. Phys. Chem. A* **1997**, *101*, 8035.